Numerical Simulation and Experimental Study of the Spiral Selector Process for Single Crystal Superalloys Part I: Starter Block Postprint

Authors: Zhang Hang, Xu Qingyan, Sun Changbo, Qi Xiang, Tang Ning, Baicheng Liu

Date: 2016-11-04T00:00:00+00:00

Abstract

The rapid development of modern aeroengines and industrial gas turbines has imposed increasingly stringent requirements on the performance of single-crystal blades. The grain selector is a critical component in single-crystal blade castings, with its key structures comprising the starter block and helical section. This study comparatively investigated, from both experimental and simulation perspectives, the variation laws of grain density and orientation in the starter block with respect to grain growth height (the height of the research position from the bottom surface of the specimen), and established design criteria for starter block parameters. EBSD (Electron Backscatter Diffraction) crystal orientation imaging technique was employed to obtain the grain morphology and orientation pole figures of starter block cross-sections; the CA-FD (Cellular Automaton-Finite Difference) method was utilized to conduct mathematical modeling and simulation of the single-crystal directional solidification process, enabling simulation calculations of the three-dimensional macroscopic temperature field and microstructure growth during solidification. From macroscopic and microscopic perspectives, the grain competitive evolution behavior during directional solidification was elucidated, revealing the fundamental laws of grain competitive growth in the starter block and providing theoretical support for starter block design.

Full Text

Numerical Simulation and Experimental Study on Grain Selection Behavior of Single Crystal Superalloy Spiral Selector I. Starter Block

ZHANG Hang[1]), **XU Qingyan**[1]), **SUN Changbo**[2]), **QI Xiang**[1]), **TANG Ning**[1]), **LIU Baicheng**[1])

[1]) Key Laboratory for Advanced Materials Processing Technology, Ministry of Education, School of Materials Science and Engineering, Tsinghua University, Beijing 100084
[2]) Shenyang Liming Aero-Engine Group Corporation Ltd., Shenyang 110043

Correspondent: XU Qingyan, associate professor, Tel: (010)62795482, Fax: (010)62773637

Supported by National Basic Research Program of China (No.2011CB706801), National Natural Science Foundation of China (No.51171089) and National Science and Technology Major Project (Nos. 2011ZX04014-052 and 2012ZX04012-011)

Abstract

The rapid development of advanced aero-engine and industrial gas turbine requires high performance of single crystal (SX) blade. The spiral selector is very important for producing SX blades, which includes a starter block and spiral part. In this research, grain density changes and orientation deviations with increasing grain growth height (the distance between the studied section and the undersurface of the sample) were investigated through experiments and simulations, and design rules for the starter block were established. EBSD orientation mapping technology was used to obtain grain morphology and orientation pole figures. Mathematical and physical models were built for the directional solidification process. Using the CA-FD method, the 3D macro temperature field of the solidification process was calculated as well as grain growth. The properties of grain competitive growth and evolution during directional solidification in the starter block were analyzed based on macro and micro modeling results, and rules for grain competitive growth were explained, which provided theoretical support for designing the starter block.

KEY WORDS spiral grain selector, starter block, numerical simulation, grain orientation, grain density

---

1.1 Simplification of Directional Solidification Process

The directional solidification process of blades is conducted in a Bridgman directional solidification furnace, which can be summarized into four main steps: heating and preheating, pouring, directional solidification withdrawal, and cooling. Therefore, the directional solidification furnace is simplified [26,27] into four parts: heating zone, radiation baffle, cooling zone, and withdrawal system, as shown in [FIGURE:1].

Single crystal blades are widely used in aviation and energy fields due to their superior high-temperature performance. These blades operate long-term in harsh environments with high temperature and high stress, and have been extensively studied from both material and processing perspectives [1-4]. Crystal defects in single crystal blades, such as stray grains and low-angle grain boundary growth, have also been investigated extensively [5-13]. These defects are directly or indirectly influenced by the grain selection process in the spiral selector.

The spiral grain selection method and the seed crystal method are two important approaches for single crystal production. The spiral grain selection method offers advantages of simple process, strong operability, and short production cycle. The key structures of the spiral selector include the starter block and the spiral part. The starter block primarily accomplishes grain chilling nucleation and competitive growth, eliminating grains with large deviation angles between the [001] preferred orientation and the heat flow direction (referred to as orientation deviation angle), ensuring a certain number of grains with small deviation angles grow into the spiral part. Starter block design failures include: too many grains entering the spiral part, causing the spiral part to fail to complete the grain selection process and resulting in double-crystal or multi-crystal defects; too few grains entering the spiral part, preventing the spiral part from performing its selection function; or grains entering the spiral part with excessively large orientation deviation angles, resulting in final single crystal structures that do not meet requirements.

Domestic and foreign scholars have conducted relevant research on spiral selectors, including analytical studies, experimental investigations, and simulation calculations on the starter block. D'Souza et al. [14] studied the effect of isothermal surface curvature on grain orientation changes during the selection process. Carter et al. [15] conducted temperature measurement experiments on the starter block and analyzed the effects of temperature gradient and cooling rate on initial competitive growth. Epishin et al. [16] investigated grain orientation distributions in the starter block. Pan et al. [17,18] performed simulations of the spiral selector and temperature measurement experiments, obtaining EBSD orientation mapping images of different sections in the starter block. Seo et al. [19] studied a transition-type selector and presented EBSD experimental results of grain orientations in the starter block. Zhou et al. [20,21] investigated competitive growth of bi-crystals and proposed a grain competition model, modifying the grain competition model proposed by Walton et al. [22]. Jiang et al. [23]

studied the grain selection process of Ni3Al-based superalloys, explaining that grain orientation relationships and phase relationships are key to the selection behavior. Meng et al. [24] systematically designed experiments to study grain density variation with height in the starter block, while using ProCast commercial software to simulate and present temperature field contour maps. Liu et al. [25] explained the competitive growth mechanism of dendrites in the starter block from the perspective of primary and secondary dendrite arm orientation distribution characteristics. Current research still has shortcomings, with most work remaining qualitative, and the mechanisms and regularities of each part of the spiral selector requiring further in-depth investigation.

This work conducts comparative studies on experimental and simulation results, explaining the grain competitive evolution process in the starter block of the spiral selector from both macro/micro temperature fields and microstructure perspectives, revealing the fundamental laws of grain competitive growth in the starter block, and proposing basic design criteria for the starter block.

1.2 Grain Competitive Growth Model Based on Temperature Field

Grain orientations at the bottom of the starter block are randomly distributed. When competitive growth continues to a certain height, the [001] orientations (preferred growth directions) of most grains become parallel or nearly parallel to the z-direction (principal stress axis direction). [FIGURE:2] shows a schematic diagram of grain competitive growth principle, assuming planar isothermal surfaces and stable crystal growth. Grains A1 and A2 have [001] orientations parallel to the z-direction, while grain B's growth direction has a certain angle with the z-direction.

The two-dimensional grain competitive growth schematic shown in [FIGURE:2a] has been analyzed in detail in studies by Walton et al. [22] and Zhou et al. [20,21]. When isothermal lines are perpendicular to the z-direction, the heat flow direction is opposite to the z-direction. Grains A1 and A2 have [001] orientations parallel to the heat flow direction, with dendrite tip growth velocities of v_1 or v_3 ($v_1 = v_3$), satisfying equation (1). Grain B's [001] orientation has a certain angle with the heat flow direction, with dendrite tip growth velocity v_2, satisfying equation (2).

Where v_1, v_2, and v_3 are the dendrite tip growth velocities of grains A1, B, and A2, respectively, satisfying $v_1 = v_2$; ΔT_1, ΔT_2, and ΔT_3 are the undercoolings at dendrite tips, with $\Delta T_1 = \Delta T_3$; ΔZ_1, ΔZ_2, and ΔZ_3 are the perpendicular distances between the solidification interface front and isothermal lines when isothermal lines are perpendicular to the z-axis, satisfying $\Delta Z_1 = \Delta Z_3$; G is the temperature gradient at the solidification interface front when isothermal lines are perpendicular to the z-axis. When each grain grows stably, equation (3) is satisfied: $_2$ is the angle between grain B's [001] orientation and the z-direction.

From equation (3), we know $v_1 < v_2$, and grains A1 and A2 grow higher than

grain B in the opposite direction of heat flow by a distance ΔZ, which remains constant.

The faster-growing grains A1 and A2 will undergo secondary arm growth and coarsening at positions higher than grain B, causing the grain boundaries between A1 and B, and between B and A2, to deflect. From [FIGURE:2a], when this growth state continues, the two grain boundaries continuously extend and expand until they intersect, eventually causing grain B's growth to be eliminated.

When isothermal lines are not perpendicular to the z-axis, the grain competitive growth situation changes, as shown in [FIGURE:2b]. When the heat flow direction has a certain angle with the z-axis (non-180°), grains A1 and A2 have a 2D ' angle between their [001] orientations and the opposite heat flow direction. Their dendrite tip growth velocity is v_1, satisfying equation (4). Grain B's [001] orientation is parallel to the heat flow direction, with dendrite tip growth velocity v_2 satisfying equation (5).

ΔZ_1', ΔZ_2', and ΔZ_3' are the perpendicular distances between the solidification interface front and isothermal lines when the heat flow direction has a 2D ' angle with the z-axis, satisfying $\Delta Z_1' = \Delta Z_3$'; G is the temperature gradient along the heat flow direction at the solidification interface front when the heat flow direction has an angle with the z-axis. When each grain grows stably, equation (6) is satisfied. From this, we know $v_2 < v_1$, and grain B grows higher than grains A1 and A2 in the opposite direction of heat flow by a distance ΔZ', which remains constant.

The faster-growing grain B will undergo secondary arm growth and coarsening at positions higher than grains A1 and A2, causing the grain boundaries between A1 and B, and between B and A2, to deflect simultaneously, as shown in [FIGURE:2b]. When this growth state continues, the two grain boundaries continuously extend and expand, eventually causing the dendrite tips of grains A1 and A2 to be suppressed by grain B's dendrite growth.

In summary, the [001] preferred orientation growth of superalloy dendrites (cubic crystal system) causes different growth heights among grains. When the isothermal surface (in 3D case) is not perpendicular to the z-axis, grains whose [001] preferred orientation is close to or parallel to the heat flow direction grow fastest along the opposite heat flow direction. Simultaneously, secondary arms at dendrite tips grow and coarsen, leading to tertiary arm growth, coarsening, and further transformation into new primary arms. Grains with large angles between their [001] preferred orientation and heat flow direction will be suppressed until completely eliminated. Therefore, inclined isothermal surfaces will favor the growth of grains with inclined [001] preferred orientation, allowing them to grow fully. As shown in [FIGURE:2b], this eventually leads to the elimination of grains with [001] preferred orientation parallel to or having small angles with the z-axis. Most selected grains have angles greater than 15° or more between their [001] preferred orientation and the z-axis.

In actual directional solidification processes, isothermal surface inclination changes the grain competitive growth process, which is unfavorable for selecting grains with [001] preferred orientation parallel to the z-direction, leading to starter block failure.

1.3 Analytical Model for Grain Density Variation

The influencing factors in actual directional solidification processes are complex and variable. This work attempts to establish an analytical model to explain the variation law of grain density with solidification height. The analytical model simplifies the actual physical process as follows: (1) Isothermal lines are horizontal with no transverse temperature gradient; (2) Within the same solidification time, the total growth lengths of different grains are equal; (3) The studied grain size is the average grain size in a statistical sense; (4) Transverse growth of secondary dendrite arms has a hindering effect on adjacent grains.

1.3.1 2D Projection of 3D Random Grain Orientations

Grains nucleate at the bottom layer through chilling, with orientations showing random distribution characteristics. Assuming infinite and continuously distributed random nucleation grains on a three-dimensional hemisphere. The optimal growth direction for cubic crystal systems is the <001> crystal direction family, with three optimal growth directions during directional solidification. Among the three optimal growth directions, the crystal orientation with the smallest angle to the z-direction is set as the [001] orientation, represented by vector λ[001]. The angle between λ[001] and the z-axis is defined as $_3$, satisfying $0 \leq {}_3 \leq {}_3$, where the maximum value in three-dimensional space is 54.7°. All grain vectors λ[001] are fixed at the coordinate origin and terminate on the surface of a unit hemisphere, as shown in [FIGURE:3a]. Vectors λ[001] with the same angle form circles (latitude lines) on the hemisphere surface. Through rotational projection, a 2D semicircle is obtained, as shown in [FIGURE:3b].

[FIGURE:3] Schematics of 2D projective picture of random distribution of grain orientation (a) random distribution of grain orientation in 3D (b) The projective picture in 2D

From the figure, the number of all λ[001] vectors distributed in space (corresponding to respective grains), denoted as A_N, is:

$$A\_N = n\_K(1 - \cos {}_3)$$

Where n_K is the grain density coefficient.

Furthermore, the proportion of grains with orientation angle satisfying $0 \leq {}_3 \leq {}_3$ is:

$$(1 - \cos {}_3) / (1 - \cos {}_3)$$

Both grains at the grain boundary position have competitive growth, and the formed grain boundary angle is within the optimal orientation angle range of the

two grains [20], as shown in [FIGURE:4]. Based on assumption (2) in Section 1.3, the angle between the grain boundary formed by grain A1 and grain B and the heat flow direction is ($\_A_1$ + $\_B$)/2. Thus, the left lateral growth amount Δl_2 of grain B is:

Δl_2 = a[tan($\_A_1$/2) - tan(($\_A_1$ + $\_B$)/2)]

During directional solidification, as grain competitive growth proceeds, grains with larger $_3$ will be continuously eliminated. The ratio of remaining grains to initial random nucleation grains can be given by equation (9):

$\_r = (1 - \cos\ _3) / (1 - \cos\ _3)$

Where $\_r$ is the ratio of remaining grains satisfying $0 \leq\ _3 \leq\ _3$ to initial random nucleation grains at a certain moment of directional solidification.

1.3.2 Grain Competitive Growth Limitation Model

During grain competitive growth, grains with large angles between their optimal growth direction and heat flow direction will gradually be eliminated. As shown in [FIGURE:4], grain A2 directly hinders grain B. According to assumption (2) in Section 1.3, the length by which grain B lags behind grain A2 in longitudinal growth is Δl_1', and under the assumed conditions, due to equal solidification time, the transverse elongation of secondary arms of grain A2 equals Δl_1', denoted as Δl_1:

Δl_1 = h[tan $\_B$ - tan(($\_A_2$ + $\_B$)/2)]

Based on the growth analysis of grain B, the growth hindrance formula can be obtained:

h[tan $\_B$ - tan(($\_A_2$ + $\_B$)/2)] = a(1/cos $\_B$ - 1)

Where h is the grain growth height; $\_\{AB\}$ is the angle between grain B's optimal orientation and the heat flow direction. The right side of equation (10) includes two components: the longitudinal growth amount of grain A2 and the longitudinal growth amount of grain B, with their difference being the transverse elongation Δl_1 of secondary arms of grain A2.

Considering the competitive growth between grain A1 and grain B, r_a is the width dimension of grain B after competitive growth; a is the average grain size when the solidification growth height is h.

From equation (12), when r_a = 0, the critical angle $\_c$ can be determined. When $\_\{AB\} \geq\ \_c$, grain B will be eliminated; when $\_\{AB\} <\ \_c$, grain B can continue to grow.

Let $\_h$ be the grain density at the cross-section when the solidification height is h, satisfying the relationship $\_h = 2/a$. Then based on equation (9), the relationship between $\_$ and a can be calculated as follows:

$a = a_0\ \_$

Where a_0 is the initial average size of grains at the bottom layer of the starter block.

According to equations (9) and (13), the relationship between average grain size a and $_3$ can be obtained as:

$a = a_0(1 - \cos\ _3\ ) / (1 - \cos\ _3\ \ )$

During directional solidification, when $a_0 = 1$ mm, the variation of grain density _h with solidification height h can be obtained according to equations (13) and (14), as shown in [FIGURE:5]. The figure shows that grain density decreases rapidly with increasing solidification height, and when the solidification height exceeds 15 mm, the rate of change of grain density with solidification height decreases.

[FIGURE:5] Analytic lines of grain density (_h) changing as solidification height (h) increasing

2 Simulation and Experimental Scheme

The structure of the spiral selector can be divided into three parts, as shown in [FIGURE:6]. The starter block and spiral part are the main components of the selector, with key design parameters including: starter block diameter ϕ, starter block height h_b, spiral part pitch h_s, spiral diameter d_s, spiral take-off angle _g, and spiral line diameter d_w.

[FIGURE:6] Structure and designing parameters of spiral selector (ϕ: diameter of starter block; h_b: height of starter block; h_s: pitch of spiral part; d_s: diameter of spiral part; _g: take-off angle; d_w: diameter of spiral line.)

The starter block structures used in actual production mainly include cylindrical and square shapes. In this study, the starter block has a cylindrical structure with h_b = 60 mm and ϕ = 15 mm.

Numerical simulation and experimental studies were conducted on the above model. The material is domestic second-generation nickel-based single crystal superalloy DD6 [28,29], with its molding pattern shown in

. Directional solidification experiments were performed using a directional solidification furnace. The starter block was sectioned at different heights, with Table 1 showing the correspondence between section numbers and distances from the bottom. The etchant used was HCl (5 mL) + HF (2 mL) + $H_2SO_4 \cdot 5H_2O$ (2 g) + H_2O (23.5 mL). Experimental grain morphologies at different cross-sections were obtained using a Zeiss (Axio Imager A1m) metallographic microscope, with full cross-section grain morphologies obtained through image stitching to statistically determine grain densities (Table 1). EBSD analysis was performed using a JEOL 6301F field emission scanning electron microscope to obtain orientation imaging maps and {001} pole figures for different grains.

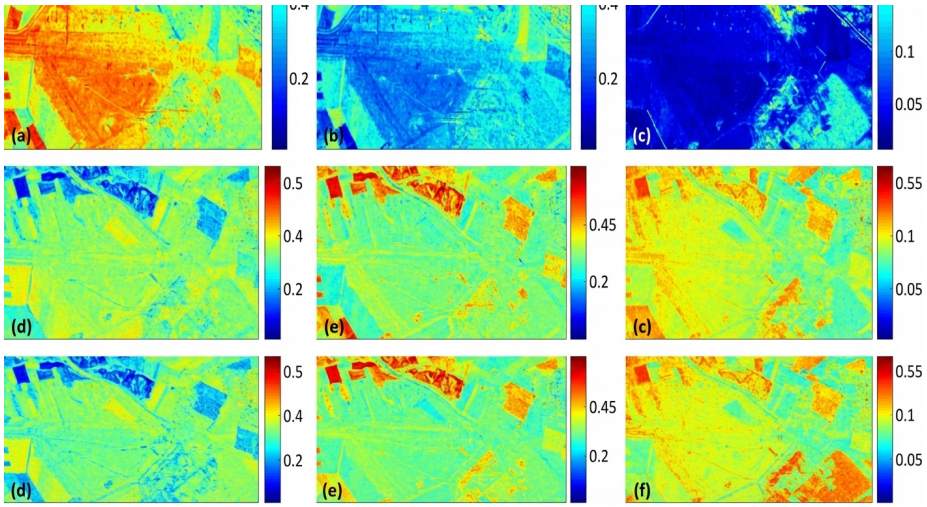

Figure 1: Figure 7

Grains consisting of dendrites with different orientations within the same cross-section have different grain numbers divided by the cross-sectional area as grain density (Table 1), as shown in [FIGURE:8a]. Within different grains, primary dendrite spacing and secondary dendrite arm orientations differ, which is used to distinguish and count different grains. Dendrite morphological characteristics are shown in [FIGURE:8b].

Schematic of statistical method for density of grains (S14 section, H=30 mm) (a) morphology of grains (b) morphologies of dendrites in the section partially

[FIGURE:9] shows the metallographic results of different cross-sections in the starter block and grain numbers at different positions, as presented in Table 1. It can be seen that as the competitive growth height increases, the number of grains decreases significantly and the average grain spacing increases. Simultaneously, as the cross-section height increases, grain orientations gradually become uniform. [FIGURE:10] shows local grain morphologies in the bottom cross-section. It is evident that different grains have significantly different orientations, resulting in obviously different etching color depths.

Due to heat radiation, the temperature gradient decreases and primary/secondary dendrite arm spacings increase. [FIGURE:11] shows dendrite morphologies at different cross-section heights. It can be observed that primary dendrite arm spacing increases significantly with increasing cross-section height. Meanwhile, secondary dendrite arms become more developed; for example, when the cross-section height exceeds that of section S13 (26 mm), secondary dendrites are very well-developed and obvious tertiary dendrites appear.

This phenomenon occurs mainly because the temperature gradient is larger at

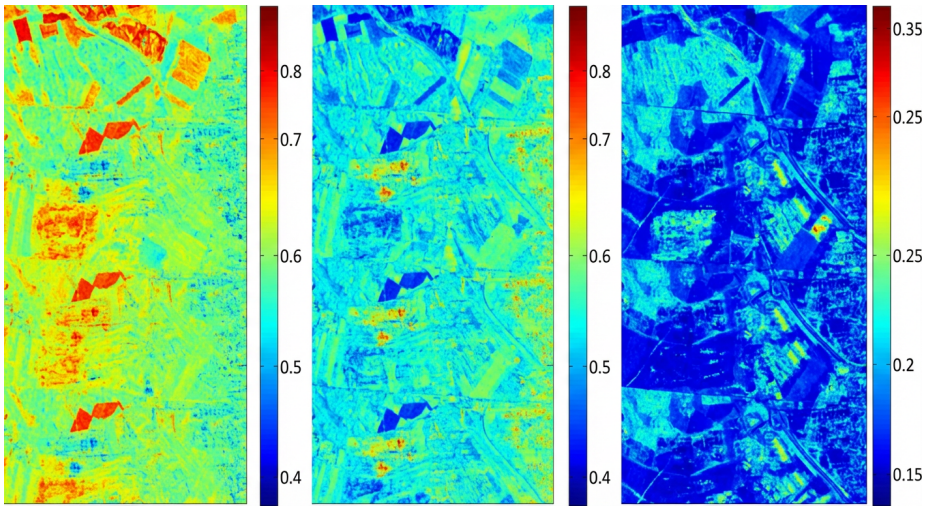

Figure 2: Figure 8

the bottom of directional solidification, resulting in intense grain competitive growth and smaller primary dendrite arm spacings. At higher cross-section positions, the heat transfer mode transitions from bottom heat conduction to lateral radiation.

In summary, as cross-section height increases, grains with larger angles between the [001] preferred orientation and heat flow direction are eliminated through competitive growth, reducing grain density.

Microstructure solidification simulations of the starter block were conducted in this study, as shown in [FIGURE:12]. Compared with experimental results in [FIGURE:9], the simulated grain distributions are basically consistent with experimental results. Statistical results of grain numbers for other cross-sections are shown in Table 1. The table shows characteristics of grain number variation with cross-section height. There are some errors between simulation and experimental results in Table 1, mainly from: (1) Model simplification error. The CA-FD model used in this study simplifies the actual physical process, describing it through mathematical equations to reflect the basic theories and laws of grain selection and competitive growth. Model simplification introduces errors between simulation and experiment. For example, section S2 in Table 1 is located at the very bottom of directional solidification, where actual solidification is completed under chilling conditions as a violently changing nonlinear process. Precisely simulating this rapid heat and momentum transfer process is difficult. This model uses an instantaneous nucleation model to ensure prediction of grain number variation during solidification under reasonable initial grain density conditions. (2) Statistical error. When the directional solidification cross-section height is large, grain [001] optimal orientations tend to be consistent. Differ-

ent grains are distinguished by different secondary arm orientations; however, grain boundaries formed by interlacing secondary arms of different grains are not clear, causing experimental statistical errors.

In summary, simulations can reflect the basic laws of grain density variation in the starter block, though the specific values are slightly smaller. This error mainly results from model simplification and grain number statistics. The CA-FD method can be used to simulate the actual physical process of directional solidification and reasonably predict solidification structure morphology, reflecting grain density variation characteristics.

3.1.2 Influence of Directional Solidification Process Parameters on Grain Density

Single crystal blade production mainly uses the directional solidification HRS method, where maintaining a horizontal and uniform temperature field is difficult to achieve [10,11,30-32]. Inclined or curved temperature field distributions vary with different directional solidification processes. Some scholars have studied the effects of withdrawal rate on curved temperature field distribution and grain inclined growth [14,32]. Liu et al. [32] believed that increasing withdrawal rate in HRS directional solidification leads to increased temperature field curvature, producing inclined isothermal line distributions. D'Souza et al. [14] studied curved isothermal lines at the solid/liquid interface front during directional solidification, pointing out that curved isothermal lines lead to a wider range of angles between selected grains' optimal orientations and the withdrawal direction.

[FIGURE:13] shows simulation results of temperature fields and structure analysis in the starter block. The figure indicates that as the solidification fraction increases, the solid/liquid interface inclination increases. When the growth interface reaches about 30 mm from the starter block bottom, the inclination angle is 22.3°, as shown in [FIGURE:13b]. When the growth interface continues to extend forward, the inclination angle becomes larger. This growth inclination originates from temperature field inclination, which is unfavorable for crystal competitive growth and selection. When the temperature field becomes inclined, it causes accelerated lateral growth of some grains, resulting in non-uniform grain sizes that seriously affect grain density distribution. Simultaneously, it may cause some coarse grains to directly enter the transition part of the selector, causing the spiral part to fail and adversely affecting grain orientation distribution.

[FIGURE:13] Simulation results of temperature fields and structure distributions (withdrawal rate: 8 mm/min) (a-c) simulations of microstructures growths and temperature distributions (d-f) slope angle of the solid/liquid surface (a, d) fs=20% (b, e) fs=50% (c, f) fs=90%

The inclined temperature field distribution and inclined microstructure growth are directly related to directional solidification conditions. Temperature field

inclination is mainly caused by two factors:

(1) Influence of mold assembly methods and multi-shell interactions.

For directional solidification processes with large furnace chambers, multi-shell methods are often used to produce small castings, such as the mold assembly scheme in this study (

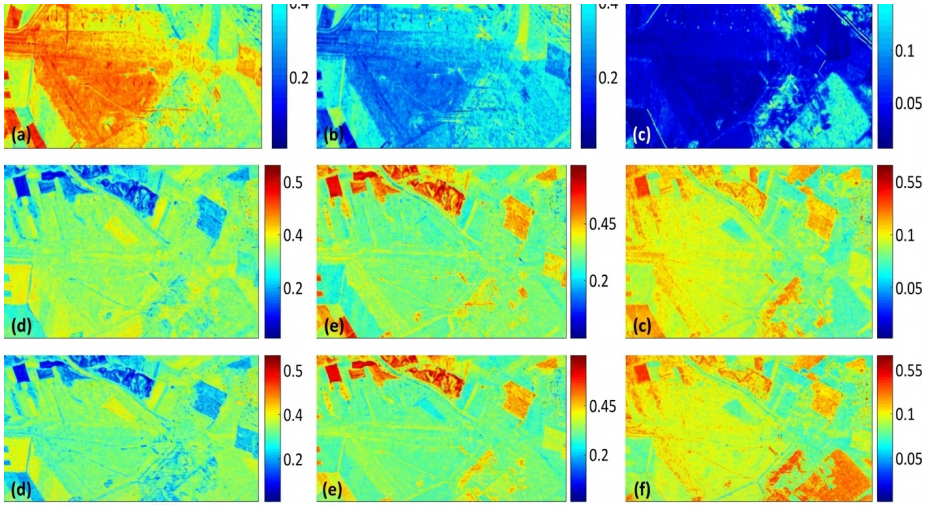

Figure 3: Figure 7

). When the casting shell is close to the furnace wall, radiation heat transfer from the directional solidification furnace wall plays an important role in the casting temperature field distribution. Generally, when the shell is withdrawn to the cooling zone of the solidification furnace ([FIGURE:1]), radiation cooling from the side wall cooling zone accelerates heat dissipation from the shell's outer surface, while the side of the casting near the furnace center dissipates heat more slowly, causing isothermal surfaces to tilt laterally from outside to inside, as shown in [FIGURE:13b] and e.

(2) Influence of withdrawal rate.

The relative magnitude between withdrawal rate and structure growth velocity determines the position of the solidification interface. When the withdrawal rate is greater than the structure growth velocity for a long time, the solid/liquid interface moves downward. If the downward position is below the baffle position, the solid/liquid interface gradually enters the cooling zone, and low-temperature radiation from the furnace side wall will dissipate heat from the shell's outer surface, causing units on the casting near the furnace wall to have lower temperatures while units near the furnace center have higher temperatures. Consequently, isothermal surfaces on the casting will tilt from the furnace wall side downward to the furnace center side, as shown in [FIGURE:13] and [FIG-

URE:14]. When this solidification condition is used for single blade casting placed at the center, a concave isothermal surface distribution will appear.

Conversely, when the withdrawal rate is less than the structure growth velocity for a long time, the solid/liquid interface moves upward. If the upward position is above the baffle position, the heating zone ([FIGURE:1]) will radiatively heat the shell, causing units on the casting near the furnace wall to have higher temperatures while units near the furnace center have lower temperatures, resulting in isothermal surfaces tilting from the furnace center side downward to the furnace wall side. When this solidification condition is used for single blade casting placed at the center, a convex isothermal surface distribution will appear.

[FIGURE:13] and [FIGURE:14] simulation results study the effects of two different withdrawal rates (5 and 8 mm/min) on temperature field distribution and subsequent structure growth inclination. The figures show that under both withdrawal rates, casting isothermal surfaces tilt from the furnace wall side downward to the furnace center side, indicating both withdrawal rates are greater than the structure growth velocity, so the solid/liquid interface is near the cooling zone. The inclination degrees differ between [FIGURE:13e,f] and [FIGURE:14b,c]. The solidification temperature field inclination at the lower withdrawal rate of 5 mm/min is significantly smaller than at 8 mm/min, which is related to the depth of the solid/liquid interface in the cooling zone. At 8 mm/min, the solid/liquid interface is deeper in the cooling zone with stronger side wall cooling radiation, thus more severe temperature field inclination. Additionally, the inclination angles in [FIGURE:13e] and [FIGURE:14a] are the same because at the initial solidification stage (fs=20%), bottom chill heat dissipation dominates, and both conditions have good unidirectional heat transfer, resulting in similar isothermal surface inclination.

From the above analysis, mold assembly methods and withdrawal rate affect structure growth by influencing temperature field distribution. According to the analysis in Section 1.2 on temperature field distribution effects on structure growth, inclined isothermal surfaces will select grains whose preferred growth direction is closest to the heat flow direction. However, these grains may have large angles with the z-axis (the blade's principal stress direction), as shown in [FIGURE:2b]. Therefore, in actual directional solidification processes, developing appropriate solidification processes (mold assembly methods and withdrawal rate) to ensure stable unidirectional heat dissipation should be emphasized in process design.

On the other hand, for the starter block directional solidification process, at the beginning stage, the melt bottom's water-cooled chill provides unidirectional heat dissipation, and isothermal surfaces are basically perpendicular to the z-axis. In the middle and later stages of directional solidification, lateral radiation heat dissipation is inevitable and also contributes to temperature field inclination. Excessive starter block height h_b will weaken bottom heat dissipation and strengthen lateral radiation heat dissipation in the middle and later stages, aggravating temperature field inclination distribution and being unfavorable for

grain competitive growth and selection of ideal grains. Therefore, selecting an appropriate starter block height to achieve certain grain density and orientation distribution is important, and the height should not be too large.

3.1.3 Variation of Grain Density with Height in Starter Block

(1) Comparison of analytical, simulation, and experimental results

Combining the analytical solution of grain density variation with height and the experimental and simulation statistical data of cross-section density variation with height in Table 1, the comparison results are shown in [FIGURE:15].

[FIGURE:15] Variation of grain density with increasing of the height of the starter block by analytic model, simulating calculation and experiment

The figure shows that analytical, simulation, and experimental results all reflect the characteristic of decreasing grain density with increasing cross-section height. However, the experimental curve shows a slower decreasing trend with larger data fluctuations because the actual heat dissipation and structure growth processes in real directional solidification are more complex. External condition influences on the solidification process cause non-uniform temperature field distribution and destroy directional heat transfer conditions, thus slowing grain competitive growth. Numerical simulation approximates real physical conditions in heat dissipation and structure growth, making simulation results more similar to experimental results, as shown in [FIGURE:15]. The analytical model starts from grain competitive growth hindrance effects and uses statistical methods to consider average grain width, but the horizontal isothermal surface assumption differs from reality, making the analytical model's directional solidification conditions more idealized and grain competitive growth more intense, resulting in the fastest grain density decrease with height in the analytical curve.

(2) Relationship between a_0 and h—influence of initial chilling solidification zone

At the beginning of directional solidification, the metal melt is chilled by the chill, nucleating and growing in an equiaxed manner, as shown in [FIGURE:16]. Equiaxed grains grow equally in all directions, with a solidification zone height of h_e. For example, in Table 1, the grain numbers of 368 for section S1 and 370 for section S2 show little change, proving that the initial 1-2 mm region is completely equiaxed nucleation and growth.

When solidification proceeds for a certain time, some equiaxed grains with faster [001] orientation growth begin to transform to columnar growth. The grain growth height at this point is set as h_c, which should satisfy $a_0 = h\_c$, where h_c is the height at which directional columnar grains begin to grow and h_e is the equiaxed zone height, as shown in [FIGURE:16].

[FIGURE:16] The height of the chilling nucleating of grains in the bottom layer

(h_c—The directional solidification height that equiaxed grains start to change to be columnar grains; h_e—the height of equiaxed zone)

From the above analysis, grain chilling nucleation and growth exist in the bottom layer of directional solidification. This zone has a height of 1-2 mm.

(3) Three zones of grain density variation in starter block

When ignoring the thickness of the initial chilling zone (1-2 mm) in directional solidification, the grain density distribution in the starter block can be divided into three zones, as shown in [FIGURE:15]. These are the exponential decreasing zone, linear decreasing zone, and stable growth zone. The figure shows that all three models basically satisfy the characteristic of rapid grain density decrease within 1-15 mm, consistent with Pan et al. [18]. Fitting the experimental results for this zone yields the function _h = 2.61exp(-0.15h) + 0.60. This zone is defined as the exponential decreasing zone. When the solidification height is in the 15-40 mm range, grain density decrease approximates a linear distribution, with the experimental fitting function _h = -0.01h + 0.60. This zone is defined as the linear decreasing zone. When solidification height exceeds 40 mm, grain density values basically stabilize, with the experimental fitting function _h = 0.20. This zone is defined as the stable growth zone.

In summary, the exponential decreasing zone of grain density in the spiral selector starter block is crucial for competitive grain selection, with a distribution height of about 15 mm. Afterward, it enters the linear decreasing zone, which further eliminates some large-angle grains. The starter block design height should be within this zone to ensure a certain number of grains eventually enter the spiral part for further elimination. Excessively high design heights cause little change in grain density while providing conditions for isothermal line and temperature gradient fluctuations, which is unfavorable for further spiral selection. Additionally, directional solidification processes also affect grain density—excessively large mold assembly radius or withdrawal rate cause isothermal line and temperature gradient inclination, which is unfavorable for grain competitive growth.

3.2.1 EBSD Experimental Results of Grain Orientation Imaging

Grain orientations in the starter block tend to concentrate as directional solidification proceeds, as shown in [FIGURE:17]. According to crystal nucleation theory, metal liquid at the bottom of directional solidification nucleates instantaneously, with grain orientations showing random distribution characteristics. As shown in [FIGURE:17a], when the sampling cross-section is 0.5 mm from the bottom, clear EBSD orientation imaging results show basically random orientation distribution. As solidification height increases, the number of grains with small angles between the [001] preferred direction and heat flow direction (referred to as orientation deviation angle) increases, while grains with large orientation deviation angles are suppressed and eliminated.

[FIGURE:17] EBSD analysis on the grain structure evolution of different sections (a) 0.5 mm (b) 6 mm (c) 12 mm (d) 24 mm

[FIGURE:18] shows {001} pole figures obtained through EBSD experiments for different cross-sections. Among them, the orientation deviation angle distributions at cross-section positions in [FIGURE:18a] and b are wide and significantly larger than 10°. When grains grow to 12 mm height, orientation deviation angles are basically less than 10°, which is basically consistent with domestic and foreign studies [15,18], as shown in [FIGURE:18c] and d.

[FIGURE:18] {001} pole figures of different sections (a) 0.5 mm (b) 6 mm (c) 12 mm (d) 24 mm

3.2.2 Comparison of Simulated and Experimental Grain Orientations

Simulation technology was used to calculate the solidification process of experimental specimens, analyzing grain orientations at different cross-sections, as shown in [FIGURE:19]. For the solidification bottom metal, [FIGURE:19a] shows that the simulation uses an instantaneous nucleation model with random grain orientations. The subsequent grain competitive growth model uses the Cellular Automaton (CA) method to simulate the actual physical process, obtaining grain orientations at different solidification growth stages.

[FIGURE:19] Simulation results of grain orientations (ϕ—the angle of normal of sample surface and grain's [001] direction) (a) 0.5 mm (b) 6 mm (c) 12 mm (d) 24 mm

Based on simulation results, statistical data of grain orientation deviation angles at different cross-section positions were calculated and compared with experiments. As shown in [FIGURE:20], when cross-section positions are low, orientation deviation angles are mainly distributed within 0-15°, but also distributed within 15°-55°. As height increases, grain competitive growth elimination occurs. When solidification height exceeds 12 mm, orientation deviation angles are mainly distributed within 0-15°, and simulation results are more concentrated within 5°, as shown in [FIGURE:20c]. This proves that intense grain competitive growth occurs within 0-12 mm of the starter block, eliminating grains with large orientation deviation angles and reducing grain density. When solidification height exceeds 24 mm, grain orientation deviation angles are mainly distributed within 0-10°, with a small amount of experimental results distributed within 10°-15°, basically meeting starter block requirements for grain orientation. Some errors exist between simulation and experiment in the small-angle range in [FIGURE:20c] and d, mainly due to simplification of the actual grain growth process in simulation and EBSD experimental precision limitations.

[FIGURE:20] Distributions of deflection angles of different sections (a) 0.5 mm (b) 6 mm (c) 12 mm (d) 24 mm

In summary, from the grain orientation perspective, the starter block should have sufficient height to successfully complete initial grain competitive growth. Increasing starter block height is meaningful for selecting grains with small orientation deviation angles. However, according to the grain density distribution conclusion above, excessively high starter block design causes insufficient grain numbers entering the spiral part. It also makes isothermal line and temperature gradient inclination more likely, which similarly affects competitive growth of grains with different deviation angles and is unfavorable for selecting grains with small deviation angles.

4 Conclusions

(1) A dendrite competitive growth model under directional solidification temperature field influence was studied, explaining the effect of temperature field on dendrite competitive growth. Based on this model, an analytical method for grain density variation with solidification height was proposed, obtaining a relationship curve between grain density and solidification height in a statistical sense.

(2) Experimental and simulation techniques were used to study the relationship between grain density/orientation and solidification height. EBSD and other methods were used to obtain experimental results of grain structures and orientation distributions at different cross-sections of the starter block. The CA-FD method was used to simulate the grain competitive growth process in the starter block, obtaining variation relationships of grain density and orientation with solidification height, which were compared with analytical and experimental results. The three results are basically consistent.

(3) Three zones of grain density distribution in the starter block were proposed: exponential decreasing zone, linear decreasing zone, and stable growth zone. These three zones describe grain density variation with solidification height and provide theoretical support for starter block height design.

References

[1] Reed R C. The Superalloys Fundamentals and Applications. UK: Cambridge University Press, 2006: 121
[2] Shi C X, Zhong Z Y. Acta Metall Sin, 2010; 46: 1281
[3] Fu H Z, Guo J J, Liu L, Li J S. Directional Solidification and Processing of Advanced Materials. Beijing: Science Press, 2008:
[4] Li J R, Xiong J C, Tang D Z. Advanced High Temperature Structural Materials and Technology. Beijing: National Defense Industry Press, 2012: 100
[5] Gandin C A, Rappaz M. Acta Metall Mater, 1994; 42: 2233
[6] Rappaz M, Gandin C A. Acta Metall Mater, 1993; 41: 345
[7] Yang X L, Lee P D, D'Souza N. JOM, 2005; 57: 40

[8] Gandin C A, Rappaz M. Acta Mater, 1997; 45: 2187
[9] JIN H, LI J, PAN D. Acta Metall Sin (Engl Lett), 2009; 22: 429
[10] Pan D, Xu Q Y, Liu B C. Sci China (Engl Lett), 2011; 54G: 851
[11] Zhang H, Xu Q Y, Tang N, Pan D, Liu B C. Sci China (Engl Lett), 2011; 54E: 3191
[12] Liu W W. Rare Met, 2011; 30: 396
[13] Yang X L, Ness D, Lee P D, D'Souza N. Mater Sci Eng: 2005; A413: 571
[14] D'Souza N, Ardakani M G, Mclean M, Shollock B A. Metall Mater Trans, 2000; 31A: 2877
[15] Carter P, Cox D C, Gandin C A, Reed R C. Mater Sci Eng, 2000; A280: 233
[16] Epishin A I, Nolze G. Crystall Rep, 2006; 51: 710
[17] Pan D, Xu Q Y, Liu B C, Li J R, Yuan H L, Jin H P. JOM, 2010; 62: 30
[18] Pan D. PhD Dissertation, Tsinghua University, Beijing, 2010
[19] Seo S M, Kim I S, Lee J H, Jo C Y, Miyahara H, Ogi K. Met Mater Int, 2009; 15: 391
[20] Zhou Y Z, Volek A, Green N R. Acta Mater, 2008; 56: 2631
[21] Zhou Y Z, Jin T, Sun X F. Acta Metall Sin, 2010; 11: 1327
[22] Walton D, Chalmers B. Trans Am Inst Min Metall Eng, 1959; 215: 447
[23] Jiang L, Li S, Han Y. Proc Eng, 2012; 27:
[24] Meng X, Lu Q, Li J, Jin T, Sun X, Zhang J, Chen Z, Wang Y, Hu Z. J Mater Sci Technol, 2012; 28: 214
[25] Liu Z Y, Lin M, Yu D, Zhou X W, Gu Y X, Fu H Z. Metall Mater Trans A, 2013; 1
[26] Yu J. PhD Dissertation, Tsinghua University, Beijing, 2007
[27] Liang Z J. PhD Dissertation, Tsinghua University, Beijing, 2003
[28] Li J R, Zhong Z G, Tang D Z, Liu S Z, Wei P, Wei P Y, Wu Z T, Huang D. In: Pollock T M, Kissinger R D, Bowman R R, Green K A, Mclean M, Oison S, Schirra J J, eds., Superalloys 2000, Warrendale, PA: TMS, 2000: 777
[29] Editorial Committee. Practical Handbook of Engineering Materials. Version 2, Beijing: China Standards Press, 2002: 771
[30] Jin H P, Li J R, Liu S Z. In: Chandra, T, Wanderka N, Reimers W, Ionescu M, eds., 6th International Conference on Processing and Manufacturing of Advanced Materials, Berlin, Germany: Trans Tech Publications Ltd, 2010: 2251
[31] Pan D, Xu Q Y, Yu J, Liu B C, Li J R, Yuan H L, Jin H P. Int J Cast Metal Res, 2008; 21: 308
[32] Liu S Z, Li J R, Tang D Z, Zhong Z G. J Mater Eng, 1999; 7: 40